Natural Resources for Human Health

visagaa publishing house

Original Research

View Article online

Check for updates

Received 05 March 2025
Revised 26 March 2025
Accepted 16 June 2026
Available Online 11 August 2026

Edited by Balamuralikrishnan Balasubramanian

KEYWORDS:
Parkinson's Disease
Coumarin
Molecular Docking
Molecular Dynamics Simulation
Mucuna pruriens
Catechol-O-Methyltransferase (COMT)

Natr Resour Human Health 2026; 6 (3): 353–366
https://doi.org/10.53365/nrfhh/224629
eISSN: 2583-1194

Hydrophobic-Driven COMT Inhibition by Coumarin from *Mucuna pruriens*: Docking, Molecular Dynamics, and Binding Free Energy Analysis in Parkinson's Disease

Mohmmad Qutboddin, Syed Sagheer Ahmed*, Bharathi Doddla Raghunathanaidu

Department of Pharmacology, Faculty of Pharmacy, Sri Adichunchanagiri College of Pharmacy, Adichunchanagiri University, Karnataka, India

ABSTRACT: The primary mechanism for dopamine degradation depends on the activity of catechol-O-methyltransferase (COMT) enzyme. The COMT inhibition may improve dopamine transmission in patients with Parkinson's disease (PD). The medicinal herb *Mucuna pruriens* (MP) protects brain cells by inhibiting COMT activity with its active components. Researchers conducted *in silico* screening to assess the efficacy of MP phytochemicals in inhibiting COMT. Overall, 13 phytoconstituents were selected through the IMPPAT 2.0 database and subjected to molecular docking (AutoDock Vina) to reveal how selected compounds interacted with the COMT crystal structure (PDB ID: 6I3D). The compounds exhibited stronger binding than both the co-crystallized ligand and the reference drug, with coumarin achieving the highest docking score of −7.6 kcal/mol, followed by linoleic acid and oleic acid at −7.5 and −7.4 kcal/mol, respectively. Coumarin binds to the COMT active site by forming hydrogen bonds with two essential amino acids, Trp143 and Ile91. The molecular dynamics simulations showed that the protein–ligand complex remained stable, with the backbone root-mean-square deviation (RMSD) fluctuating between 1.3 and 1.6 Å. The root-mean-square fluctuation (RMSF) results, combined with the protein–ligand interactions, demonstrated that the ligand maintained stable contact through binding interactions, including both hydrophobic interactions and water-mediated hydrogen bonds with Glu90. The molecular mechanics–generalized born surface area (MM–GBSA) determined that the system achieved a favorable binding free energy of −75.19 ± 4.96 kcal/mol, driven by hydrophobic stabilization via van der Waals and lipophilic interactions.: The natural compound Coumarin from MP shows potential as a COMT inhibitor for the treatment of PD.

* Corresponding author.
E-mail address: sagheer@accp.co.in (Syed Sagheer Ahmed)

GRAPHICAL ABSTRACT

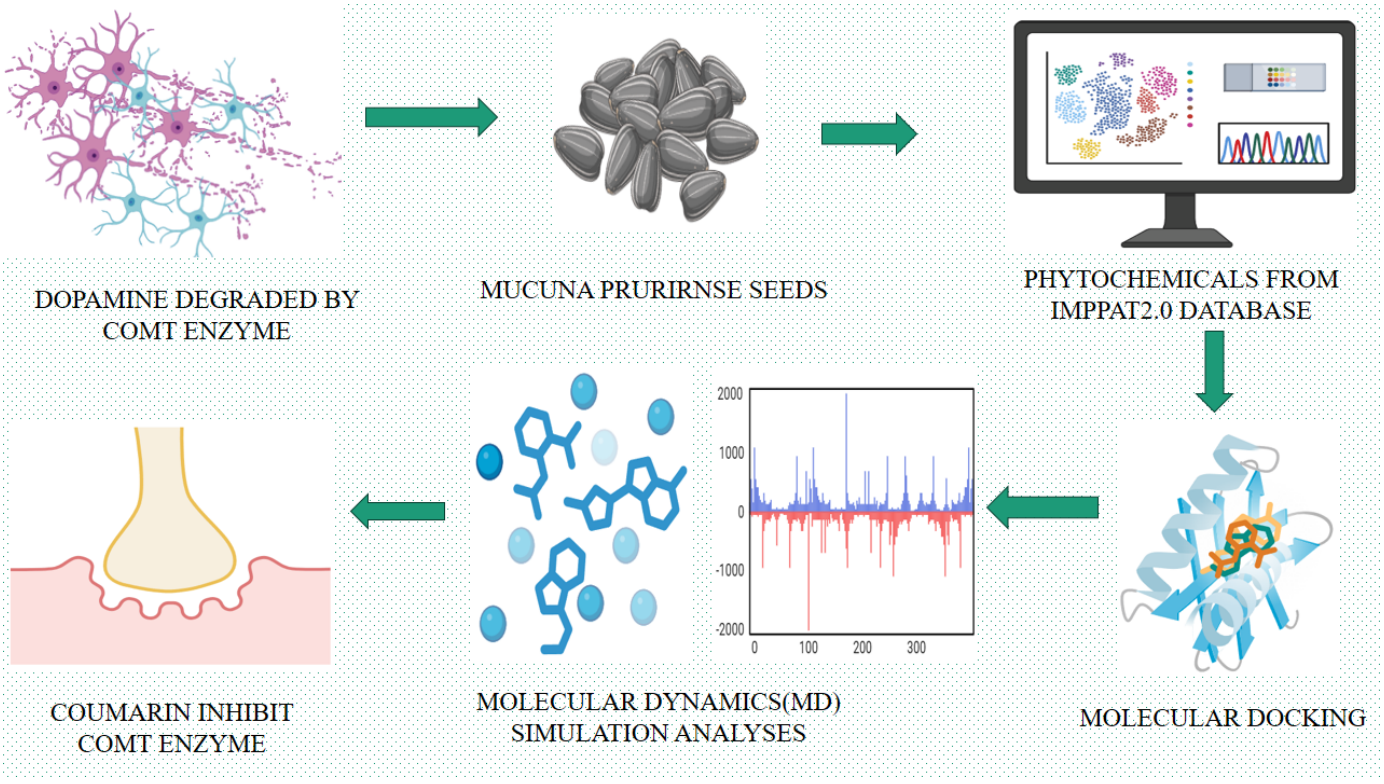

1. INTRODUCTION

Parkinson's disease (PD) represents the second most prevalent neurodegenerative condition and develops due to the progressive degeneration of dopaminergic neurons in the substantia nigra (SN) region of the brain (Lev et al., 2003; Singh & Dikshit, 2007). It is a rapidly growing global health concern, with recent estimates indicating that more than 10 million people worldwide are currently living with the disease, and its prevalence is expected to increase substantially due to population aging (Dorsey et al., 2018; GBD 2021, Parkinson's Disease Collaborators, 2024).

The primary symptoms of PD include resting tremors, stiffness, bradykinesia, and postural instability (Balestrino & Schapira, 2020). Dopamine depletion and norepinephrine deficiency in PD result in multiple symptoms, including bradykinesia, tremors, speech difficulties (dysarthria), rigidity, and cognitive impairment (Kalia & Lang, 2015; Poewe et al., 2017). Extensive research has been conducted, but the specific cause of the disease remains undetermined (Poewe et al., 2017). The disease progression occurs with the formation of Lewy bodies through alpha-synuclein protein aggregation (Spillantini et al., 1997; Wong & Krainc, 2017). PD has two primary forms: (1) brain-first PD, which starts with alpha-synuclein pathology in the brain, and (2) body-first PD, which starts in the peripheral nervous system, particularly in the gut, before spreading through the vagus nerve or bloodstream (Horsager et al., 2020).

Today, pharmaceutical treatment of PD relies on four main medication categories, which include levodopa (L-DOPA) with decarboxylase inhibitors plus dopamine agonists and catechol-O-methyltransferase (COMT) inhibitors and monoamine oxidase-B (MAO-B) inhibitors (Balestrino & Schapira, 2020; Kalia & Lang, 2015). The main role of COMT inhibitors is to prevent the body from breaking down L-DOPA outside the brain, which results in extended dopamine effects and improved therapeutic outcomes (Männistö & Kaakkola, 1999).

Growing interest in plant-based therapies has encouraged exploration of natural alternatives. *Mucuna pruriens* (MP), commonly known as velvet bean, belongs to the Fabaceae family and is widely distributed across tropical regions (Hettiarachchi and Gunathilake, 2023; Lampariello et al., 2012). The people of Asia, Africa, and the Americas have traditionally used the plant as food and for its medicinal

properties. The seeds of the plant contain high amounts of L-DOPA, which serves as a direct precursor for dopamine synthesis. *M. pruriens* seeds have been part of traditional Indian medicine for more than 2000 years as a PD treatment (Katzenschlager et al., 2004; Manyam, 1995). The seeds possess multiple pharmacological properties, including antioxidant, anti-inflammatory, hypolipidemic, and hypoglycaemic activities (Sathiyanarayanan & Arulmozhi, 2007). The biological activities of these substances appear to provide both neuroprotection and help alleviate symptoms.

M. pruriens contains natural L-DOPA, which has the potential to boost dopaminergic activity by inhibiting COMT enzyme function (Manyam, 1995). The inhibition of COMT reduces dopamine breakdown and improves L-DOPA absorption, and it also has the potential to improve PD treatment outcomes. The enzyme COMT plays a critical role in dopamine metabolism by transferring methyl groups to catechol substrates, which then undergo metabolic conversion (Männistö & Kaakkola, 1999). The process of blocking COMT activity becomes necessary as it increases the dopamine levels in the brain and extends the duration of the therapeutic effects of L-DOPA.

The discovery of natural COMT inhibitors from MP provides a complementary treatment method for patients receiving pharmacological treatments. *In silico* techniques such as molecular docking, molecular dynamics (MD) simulations, and binding free energy calculations serve as powerful computational tools in predicting ligand–protein interactions and enzyme inhibition mechanisms at the atomic level (Hollingsworth & Dror, 2018; Lionta et al., 2014). The present study investigates how MP seed phytoconstituents inhibit COMT through molecular docking, MD simulations, and binding free energy analysis to discover natural substances that can enhance PD treatment.

2. MATERIALS AND METHODS

2.1. Phytoconstituent selection and preparation

The researchers selected phytoconstituents present in MD based on their reported presence in the IMPPAT 2.0 (Indian Medicinal Plants, Phytochemistry and Therapeutics) database, a collection of phytochemical and ethnopharmacological data. The selected compounds demonstrated their structural diversity by representation of different chemical classes, including fatty acids, indole derivatives, alkaloids, and phenolic compounds. In addition, the drug-likeness of the selected phytoconstituents was evaluated based on Lipinski's rule of five, which predicts oral bioavailability of compounds. According to this rule, compounds are more likely to exhibit good permeability and absorption when they satisfy the following criteria: molecular weight ≤ 500 Da, octanol–water partition coefficient (LogP) ≤ 5, hydrogen bond donors ≤ 5, and hydrogen bond acceptors ≤ 10 (Lipinski et al., 2001). Compounds with minimal or no violations were considered suitable for further computational analysis.

The three-dimensional (3D) structures of the selected phytoconstituents were obtained from the IMPPAT 2.0 database in the Structure Data File (SDF) format. Ligand preparation was performed to generate stable energy configurations that served as the foundation for molecular docking experiments. The researchers conducted energy minimization for each phytoconstituent using the **Merck Molecular Force Field (MMFF94)** to eliminate all steric clashes and achieve the most accurate molecular shape. The ligands were converted to PDBQT format after energy minimization, which included assigning atom types and partial charges required for AutoDock Vina v1.2.0 docking. The research team used all synthesized compounds for molecular docking studies, which were conducted under identical computational conditions (Mohanraj et al., 2018).

2.2. Protein selection and preparation

The 3D crystal structure of the target enzyme was obtained from the Protein Data Bank (PDB) using accession ID 6I3D. The protein structure was prepared for docking by removing all nonessential molecules, including crystallographic water and co-crystallized ligands. The polar hydrogen atoms were added to the structure, and the partial charges were distributed. The protein structure was saved in PDBQT format (6I3D.pdbqt) for molecular docking research (Berman et al., 2000).

2.3. Grid box generation

The researchers established the docking search area by constructing a grid box that included the active site of the target protein. The grid box parameters were chosen to ensure full coverage of the binding pocket while allowing enough flexibility for ligand sampling across various molecular configurations. The grid box parameters have been specified as follows:

2.3.1. Grid center coordinates

- center_x = 2.70
- center_y = 16.06
- center_z = 69.39

2.3.2. Grid box dimensions

- size_x = 20 Å
- size_y = 20 Å
- size_z = 20 Å

Energy range: 4 kcal/mol; Exhaustiveness: 8.

The aforementioned rules and tests were consistently applied during the local docking screening to achieve accurate force calculations.

2.4. Molecular docking procedure

The researchers utilized AutoDock Vina v1.2.0 to conduct molecular docking experiments, which involved predicting ligand binding shapes and their associated binding strengths using its scoring system and random optimization techniques. Separate docking experiments were carried out for each synthesized ligand, with each ligand being docked into the specified grid box of the target protein. Multiple binding shapes were generated for each ligand, and the shape with the lowest binding energy (kcal/mol) was chosen for further interaction studies. (Trott & Olson, 2010)

2.5. Visualization and interaction analysis

The researchers utilized the BIOVIA Discovery Visualizer software to conduct visualization and interaction analysis following docking. They developed two-dimensional (2D) interaction diagrams to illustrate all hydrogen bonds, π–π stacking, π–alkyl interactions, and other noncovalent contacts that ligands establish with the active-site residues of the target protein.

2.6. Molecular dynamics simulation

The Desmond module, part of the Schrödinger software suite (**Schrödinger Release 2021-4**), was used to perform an MD simulation to evaluate the dynamic stability of the protein–ligand complex over 200 nanoseconds. The complex system was built using System Builder as the base, since it required solvating the complex in an orthorhombic box with the TIP3P water model while maintaining a buffer zone of 10 Å from the protein boundary. System neutrality was achieved by adding the necessary counterions, together with 0.15 M NaCl, which simulated the ionic strength found in natural body fluids. The system underwent energy minimization using the **Optimized Potentials for Liquid Simulations (OPLS)** force field before entering the **NVT (constant Number of particles, Volume, and Temperature)** and **NPT ensembles (constant Number of particles, Pressure, and Temperature)** for a gradual equilibration. The production MD simulation was run for 100 nanoseconds at 300 K and atmospheric pressure, with NPT control using the Nose-Hoover thermostat and the Martyna-Tobias-Klein barostat. The research team recorded their trajectories at regular intervals for evaluating the structural stability and interaction persistence via RMSD and RMSF, hydrogen bonding, and other dynamic parameters (Bowers et al., 2006).

3. RESULTS

3.1. Molecular docking analysis of *Mucuna pruriens* phytoconstituents against COMT

Scientists used molecular docking techniques to assess the binding affinity of MP phytoconstituents for the COMT protein. The research team examined 13 phytoconstituents using docking to evaluate their binding affinity relative to the co-crystallized ligand and the reference medication, as shown in Table 1. Docking scores are reported in kcal/mol, with lower scores indicating stronger binding. The tested compounds showed several docking scores that exceeded the co-crystal ligand value of −5.2 kcal/mol and the reference medication value of −4.4 kcal/mol. Coumarin achieved the highest docking score of −7.6 kcal/mol among all the substances tested. It was followed by linoleic acid with a score

Table 1
Docking scores and hydrogen bond interactions of selected phytoconstituents from *Mucuna pruriens* against Catechol-O-methyltransferase (COMT, PDB ID: 6I3D).

SN	Phytoconstituents	Docking Score (kcal/mol)	No. of H-bonds
1	Myristic acid	−7.3	3
2	Bufotenine	−6.4	1
3	Tryptamine	−6.2	2
4	N,N-Dimethyl-5-methoxytryptamine	−6.5	1
5	Coumarin	−7.6	–
6	Choline	−3.0	1
7	Stearic acid	−6.2	–
8	Serotonin	−6.0	–
9	N,N-Dimethyltryptamine	−6.3	1
10	Palmitic acid	−6.8	4
11	Oleic acid	−7.4	1
12	Beta-Sitosterol	−7.0	–
13	Linoleic acid	−7.5	–
14	Co-crystal ligand	−5.2	5
15	Reference drug	−4.4	–

of −7.5 kcal/mol, oleic acid at −7.4 kcal/mol, and myristic acid at −7.3 kcal/mol. The results show that these phytoconstituents bind more strongly to the COMT binding site than the reference ligands. The fatty acid–derived phytoconstituents showed moderate to high docking scores, with palmitic acid (−6.8 kcal/mol) and oleic acid, linoleic acid, myristic acid, and stearic acid (−6.2 kcal/mol). Palmitic acid produced the most hydrogen bonds with four bonds. Myristic acid and oleic acid formed three and one hydrogen bonds, respectively, demonstrating different ways of forming polar interactions despite their similar binding strengths.

Indole and tryptamine derivatives, including N, N-dimethyl-5-methoxytryptamine (−6.5 kcal/mol), N, N-dimethyltryptamine (−6.3 kcal/mol), tryptamine (−6.2 kcal/mol), bufotenine (−6.4 kcal/mol), and serotonin (−6.0 kcal/mol), demonstrated modest docking scores. The compounds formed between zero and two hydrogen bonds, which showed limited polar interactions compared to both fatty acids and the co-crystal ligand. The docking score for choline reached its lowest value of −3.0 kcal/mol because it formed one hydrogen bond with the COMT active site, yet maintained a weak binding affinity. The co-crystal ligand formed five hydrogen bonds, yet most phytoconstituents showed better docking performance than it did. The reference medication had the least favorable docking score and failed to form hydrogen bonds under the specified docking conditions. This may be attributed to its improper orientation within the active site or the absence of suitable hydrogen bond donor and acceptor groups, which limited its interaction with key catalytic residues. Additionally, steric hindrance and suboptimal binding conformation may have contributed to its reduced binding affinity.

3.2. Coumarin–COMT interaction

The three-dimensional molecular interaction of coumarin docked at the COMT active site is shown in Figure 1. The analysis of interactions showed that the binding pocket contained multiple π-mediated and hydrophobic interactions. The Trp143 residue showed two types of interactions with coumarin, the π–π and π–alkyl interactions at distances of 4.92 and 5.11 Å, respectively. The researchers discovered additional hydrophobic interactions with Ile91 at two distance points, 3.76 and 3.98 Å. The ligand was connected with Gly66 and His142 at distances of 5.02 and 4.92 Å. The binding orientation of coumarin within the COMT active site can be defined through the interaction.

3.3. Linoleic acid–COMT interaction

The 2D diagram in Figure 2 demonstrates the interaction between linoleic acid and COMT. The interaction profile

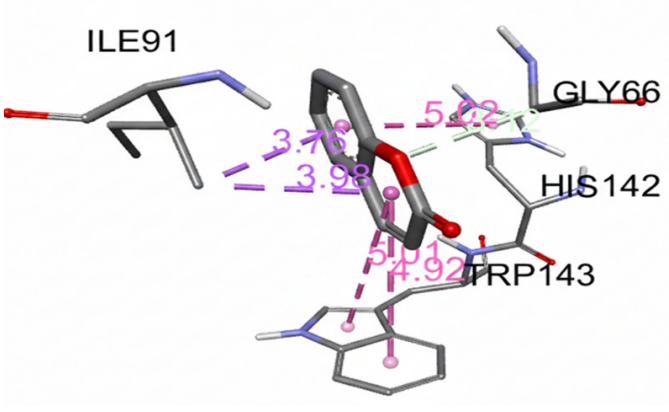

Figure 1. Three-dimensional (3D) molecular interaction of coumarin with catechol-O-methyltransferase (COMT) enzyme obtained from molecular docking analysis. The figure illustrates the binding orientation of coumarin within the active site of COMT, highlighting key amino acid residues involved in ligand stabilization, including Trp143 and Ile91. Noncovalent interactions such as π–π stacking and hydrophobic interactions are shown, which contribute to binding affinity.

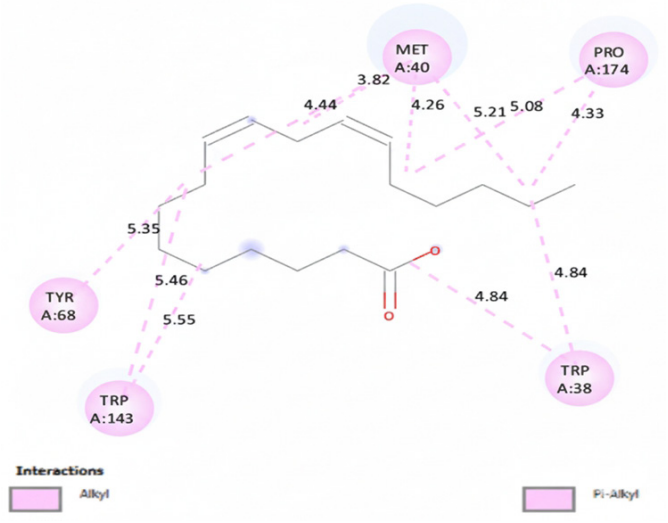

Figure 2. Two-dimensional (2D) interaction diagram of linoleic acid bound to the catechol-O-methyltransferase (COMT) active site. The figure represents hydrophobic interactions, including alkyl and π–alkyl contacts, between linoleic acid and surrounding amino acid residues such as Met40, Pro174, and Trp143. No conventional hydrogen bonds are observed, indicating a predominantly hydrophobic mode of binding.

shows that the binding site of COMT is mainly occupied by alkyl and π–alkyl connections to its surrounding residues. Linoleic acid established hydrophobic contacts with Met40 at distances of 3.82 and 4.26 Å, and with Pro174 at 4.33, 5.08, and 5.21 Å. The study found extra alkyl bonding, which occurred with Trp38 at a distance of 4.84 Å and with Trp143 at 5.46 and 5.55 Å. The ligand formed additional bonds with Tyr68, which showed interaction distances of 5.35 and 5.46 Å. The linoleic acid–COMT complex showed no evidence of conventional hydrogen bond interactions.

3.4. Co-crystal ligand–COMT interaction

Figure 3 displays the 2D molecular interaction profile, which shows how the co-crystal ligand interacts with the COMT active site. The interaction map shows that active site residues form multiple established hydrogen bonds together with carbon–hydrogen bond connections. Conventional hydrogen bonds were observed between the ligand and Ser119 (2.93 Å), Gly66 (2.77 Å), Asp141 (2.75 Å), and Asn170 (3.39 Å). Additional carbon–hydrogen bond interactions were identified with His142 (3.21 Å) and Met40 (2.88 Å). The ligand also exhibited a π–cation interaction with Lys144 (3.59 Å) and π–alkyl interactions with Pro174 at distances of 4.28 and 5.23 Å. These association occurrences describe the binding pose of the co-crystalline ligand within the COMT-binding pocket.

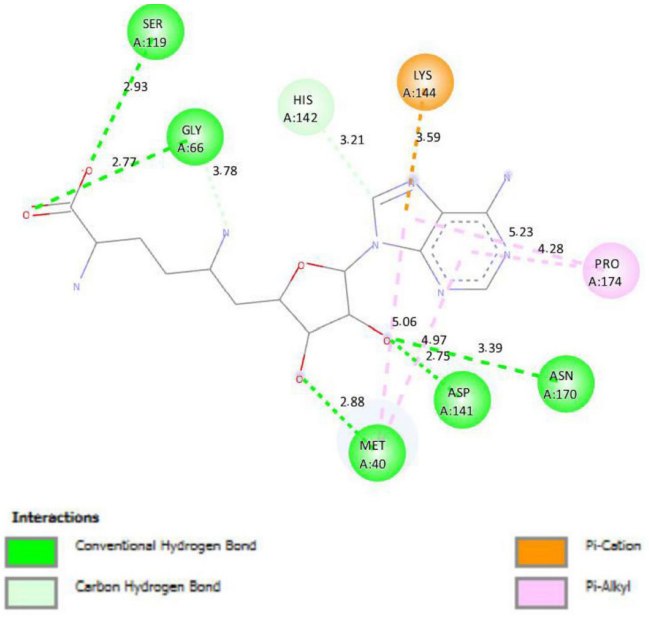

Figure 3. Two-dimensional (2D) molecular interaction profile of the co-crystallized ligand with the catechol-O-methyltransferase (COMT) enzyme. The diagram shows multiple conventional hydrogen bonds (e.g., Ser119, Gly66, Asp141, and Asn170), along with additional interactions such as π–cation and π–alkyl contacts, demonstrating strong polar and electrostatic contributions to ligand binding.

3.5. Reference drug–COMT interaction

The 2D molecular interaction diagram of the reference drug docked into the COMT active site is presented in Figure 4. The interaction analysis revealed van der Waals interactions with Trp143 and Met40, along with a carbon–hydrogen bond involving Pro174 (3.21 Å). The ligand formed a π–lone pair interaction with Asp141 at 2.84 Å distance, and an amide–π stacking interaction with His142 was found at 5.22 Å distance. Additional alkyl and π–alkyl interactions were identified with Met40 and Pro174, with interaction distances of 3.87 and 3.99 Å, respectively. The interactions present in this study demonstrate how the reference drug binds to the COMT active site.

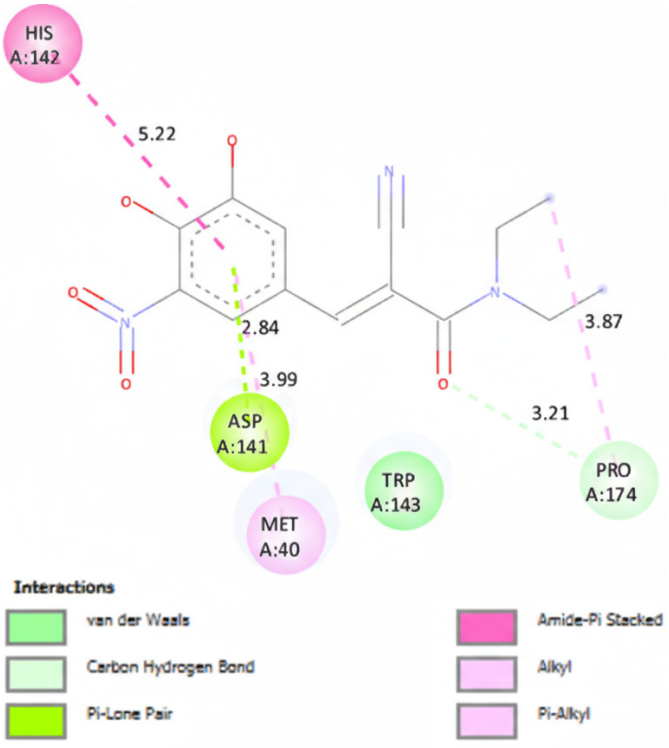

Figure 4. Two-dimensional (2D) molecular interaction diagram of the reference drug within the catechol-O-methyltransferase (COMT) binding pocket. The interaction map highlights van der Waals forces, carbon–hydrogen bonds, π–lone pair interactions, and π–alkyl contacts with residues such as Met40, Pro174, Asp141, and His142, indicating comparatively weaker binding interactions.

3.6. Molecular dynamics simulation

3.6.1. Root mean square deviation (RMSD)

The analysis of ligand flexibility (Figure 5) revealed very small internal motion of the ligand due to the RMSF below 0.05 Å. The active site movement restrictions of the protein structure resulted in RMSF value measurements of about 1.45–1.55 Å, and these restrictions occurred without any structural changes to the ligand. The protein RMSF analysis demonstrated system stability; the majority of the residues showed only small movements under 0.4–0.8 Å, with loop regions and terminal residues exhibiting greater movement, which measured from 1.5 to 1.9 Å and 3.0 Å, respectively. After all, this pattern occurs in solvated protein systems and does not result from ligand instability.

3.6.2. Root mean square fluctuation (RMSF)

The analysis of ligand flexibility (Figure 6) indicated very little internal movement, with RMSF values being less than 0.05 Å when aligned with itself. The RMSF values ranged from 1.45 to 1.55 Å during protein alignment, which indicated slight positional changes to the active site rather than any structural deformation of the ligand. The RMSF analysis of the protein in Figure 7 confirmed system stability as most residues displayed small movements ranging from 0.4 to 0.8 Å. Proteins in solution usually display increased mobility in loop regions, which show measurements between 1.5 and 1.9 Å, and terminal residues, which show measurements around 3.0 Å, and this observation does not connect to any instability brought by the ligand.

3.7. Ligand properties

The physicochemical properties of the ligands delivered identical results during testing throughout the simulation. The ligands showed an RMSD range of 0.08 to 0.15 Å while maintaining a radius of gyration between 2.25 and 2.30 Å. The MolSA values were recorded between 148 and 152 Å², whereas the polar surface area maintained a stable range of 63–67 Å². The SASA variations, spanning from 50 to 300 Å², indicated changes in the ligand's solvent exposure while it retained its compact form. Trajectory analysis revealed the absence of hydrogen bonds between the molecules. Experimental findings indicate that the Coumarin–COMT complex exhibits robust structural stability, controlled ligand dynamics, and effective binding properties throughout the MD simulation (Figure 8).

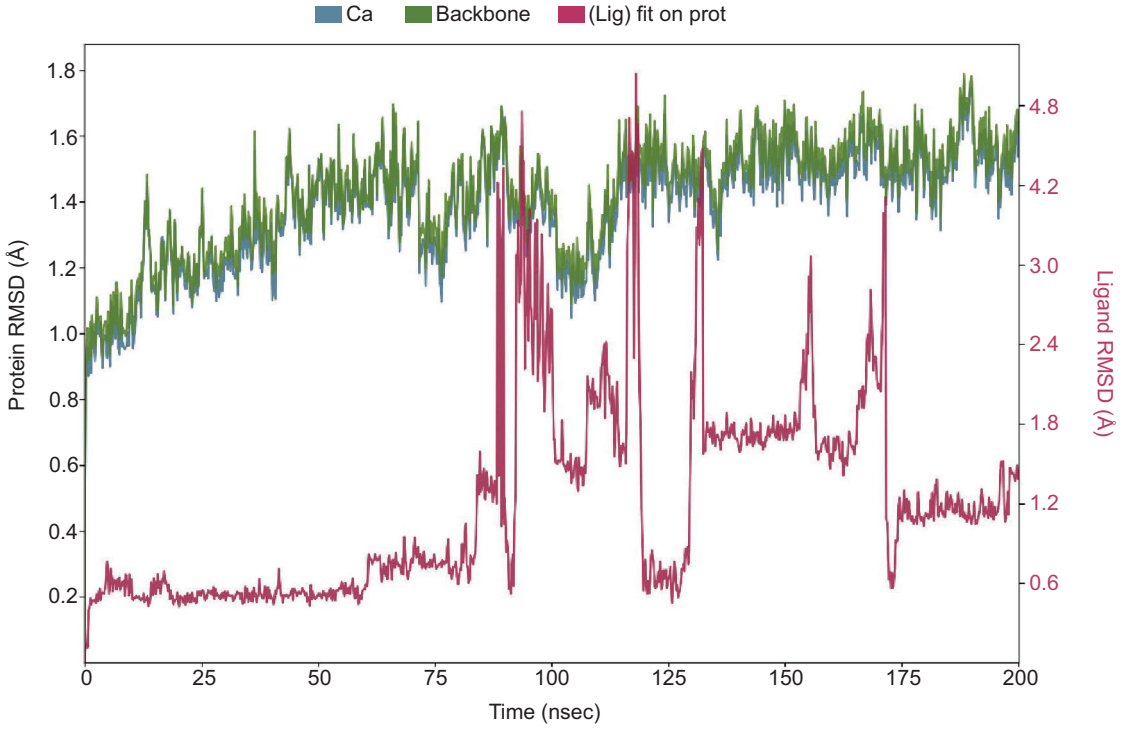

Figure 5. Root mean square deviation (RMSD) plot of the coumarin–COMT complex obtained from molecular dynamics simulation over 100 ns. RMSD represents the deviation of the protein backbone atoms over time, indicating the structural stability of the protein–ligand complex during the simulation.

Figure 6. Root mean square fluctuation (RMSF) plot of the ligand (coumarin) during the molecular dynamics simulation. RMSF indicates the flexibility and internal motion of the ligand atoms throughout the simulation period.

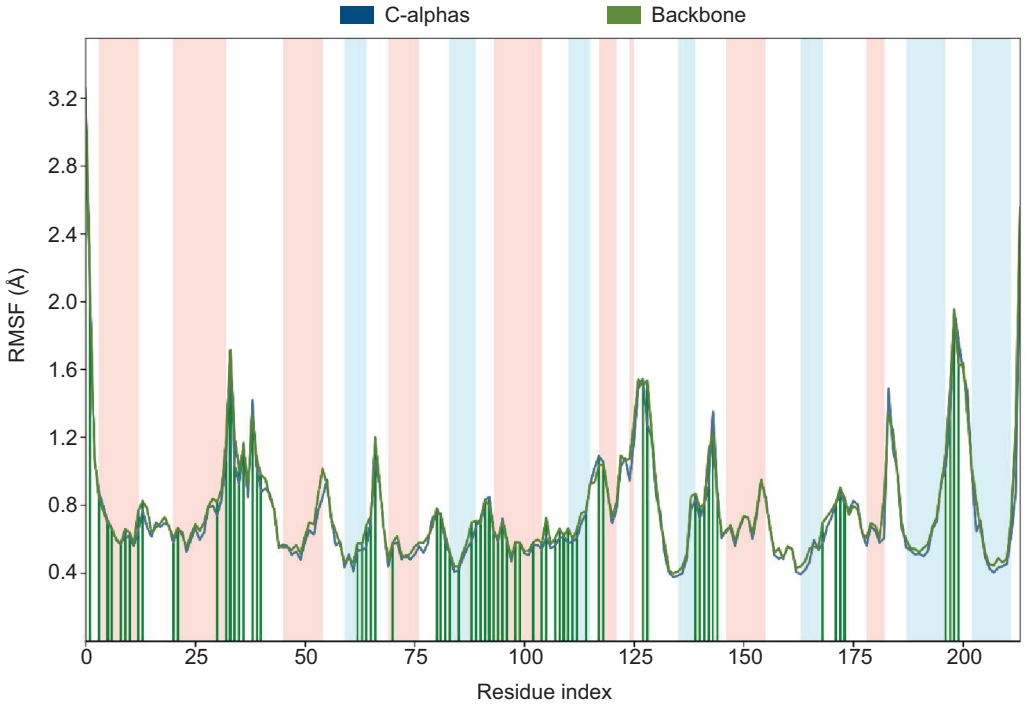

Figure 7. Root mean square fluctuation (RMSF) plot of the catechol-O-methyltransferase (COMT) protein residues. The plot shows residue-wise flexibility, where lower fluctuations indicate stable regions, and higher fluctuations correspond to flexible loop and terminal regions.

3.8. Protein–ligand interaction

The analysis of protein–ligand interactions reveals that Coumarin consistently forms stable and specific contacts with the active site residues of COMT throughout the simulation.

The 2D interaction map in Figure 9 shows that the carbonyl oxygen of Coumarin formed a water-mediated hydrogen bond with Glu90, which lasted for approximately 6% of the simulation time, while hydrophobic proximity with Met40 further supports ligand anchoring. The protein–ligand contact histogram in Figure 10 shows that multiple residues

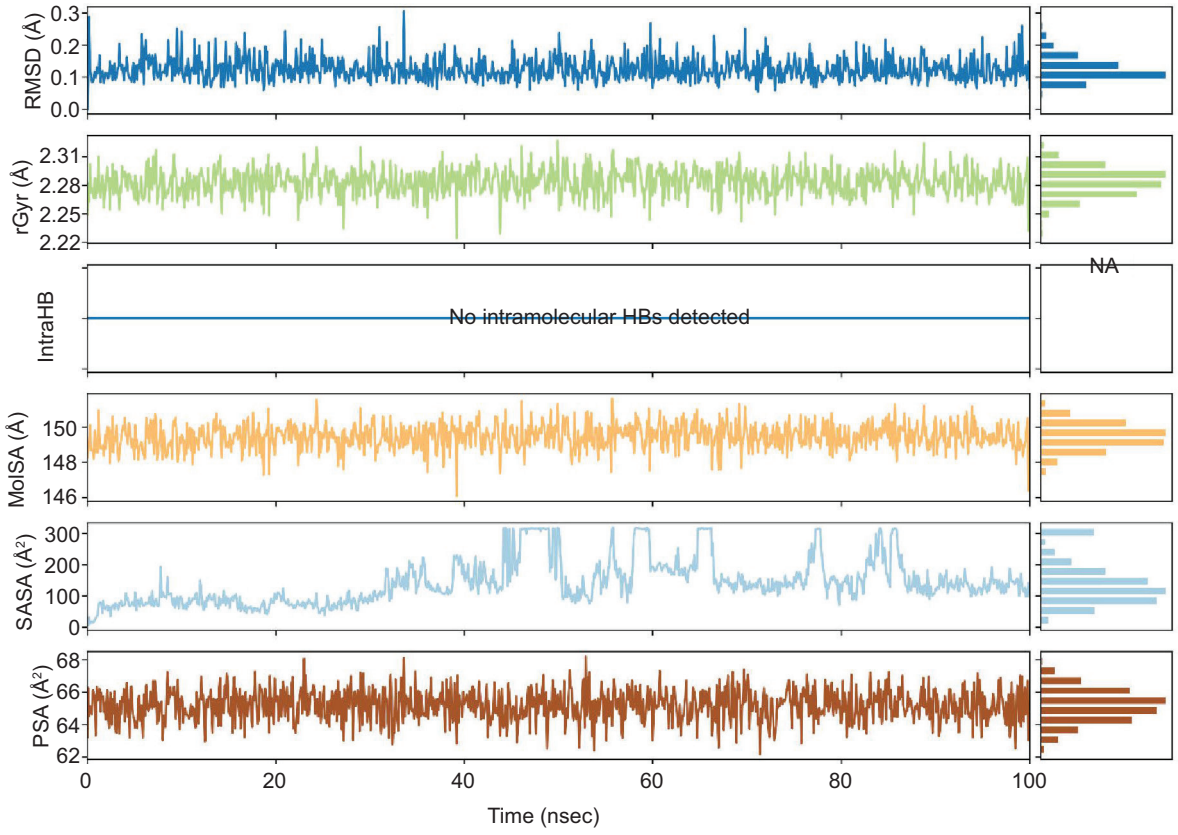

Figure 8. Analysis of ligand properties during molecular dynamics simulation, including root mean square deviation (RMSD), radius of gyration (Rg), molecular surface area (MolSA), solvent-accessible surface area (SASA), and polar surface area (PSA). These parameters describe ligand stability, compactness, and solvent exposure throughout the simulation.

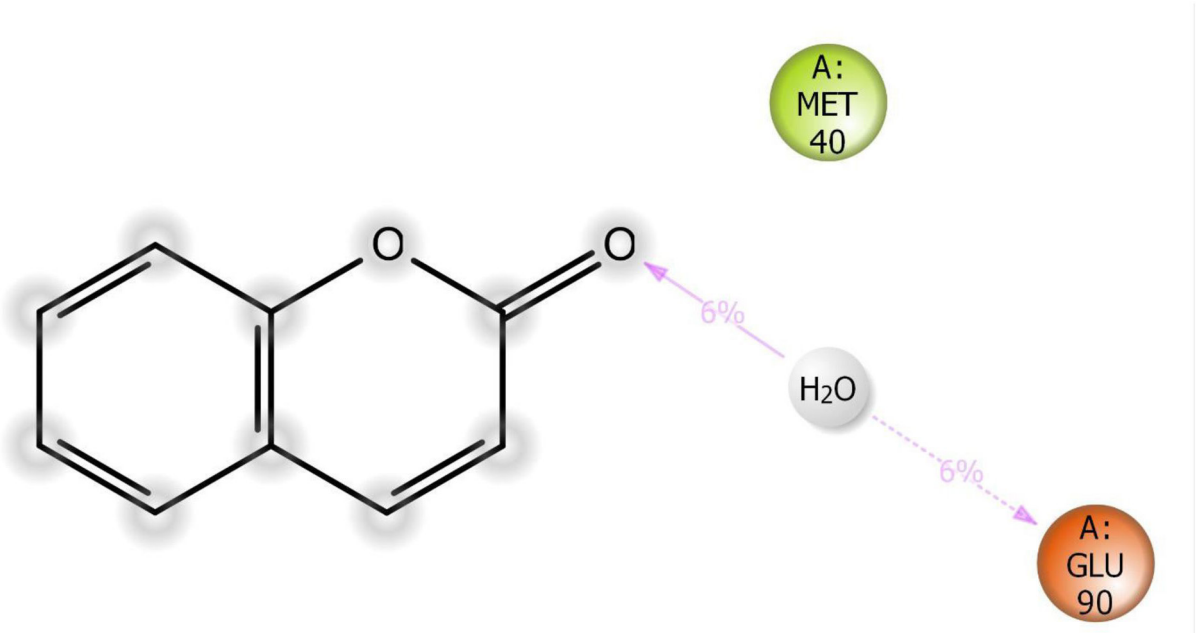

Figure 9. Protein–ligand interaction diagram showing key contacts between coumarin and catechol-O-methyltransferase (COMT) active site residues during molecular dynamics simulation. The figure highlights hydrogen bonding, hydrophobic interactions, and water-mediated contacts that contribute to binding stability.

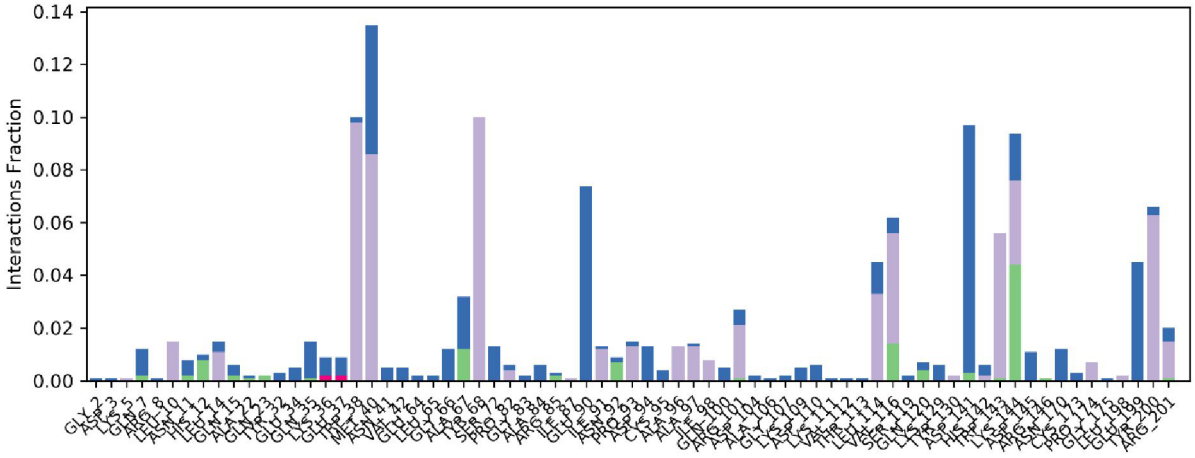

Figure 10. Protein–ligand contact histogram representing the frequency of interactions between coumarin and catechol-O-methyltransferase (COMT) residues throughout the simulation. The interaction fraction indicates how often specific residues participate in binding over the simulation time.

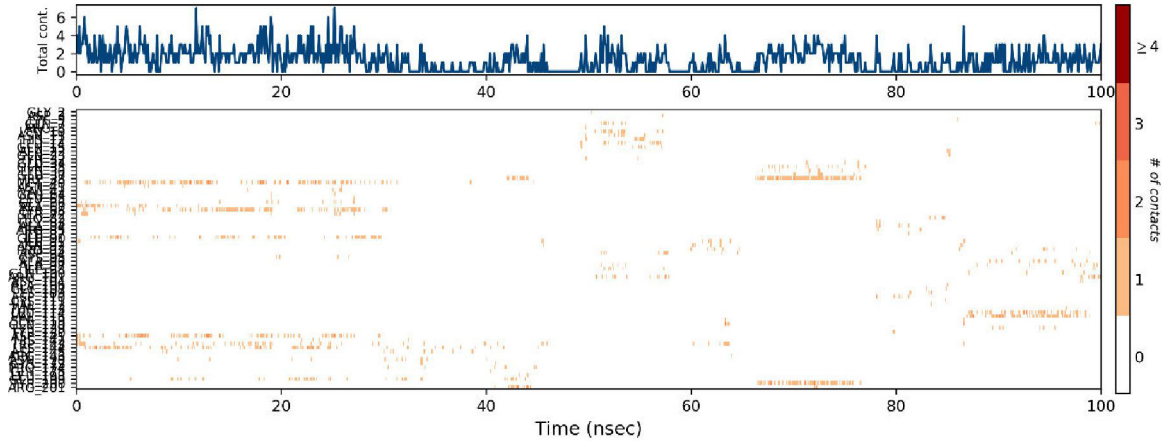

Figure 11. Protein–ligand contact timeline showing the temporal evolution of interactions between coumarin and catechol-O-methyltransferase (COMT) over the 100 ns simulation. The variation in the number of contacts per frame reflects the persistence and stability of binding interactions.

maintain consistent binding, while important interacting residues display interaction fractions between 6 and 14%, which indicates that they make repeated contact instead of brief contact. The contact timeline in Figure 11 shows that these interactions remain active because the number of contacts varies between approximately 1 contact and 4 contacts for each frame during the 100 nanosecond trajectory. Notably, interaction events are distributed across the simulation rather than clustered in short intervals, which demonstrates that binding stability lasts for an extended period. The stable and well-maintained Coumarin–COMT interaction throughout the MD simulation is confirmed by contact frequency, interaction persistence, and water-mediated hydrogen bonding.

3.9. MM–GBSA energy calculation

The binding free energy results from molecular mechanics–generalized born surface area (MM–GBSA) analysis show that Coumarin–COMT complex exhibits favorable binding free energy with an average binding energy of ΔGbind = −75.19 ± 4.96 kcal/mol, as shown in Figure 12. The interaction relies on nonpolar/dispersion forces as the main component, which is demonstrated by the extremely negative van der Waals term value (ΔG_vdW = −49.93 ± 4.94 kcal/mol) together with the substantial lipophilic contribution of (ΔG_lipophilic = −29.91 ± 5.10 kcal/mol), which indicates hydrophobic packing functions as the primary stabilizing

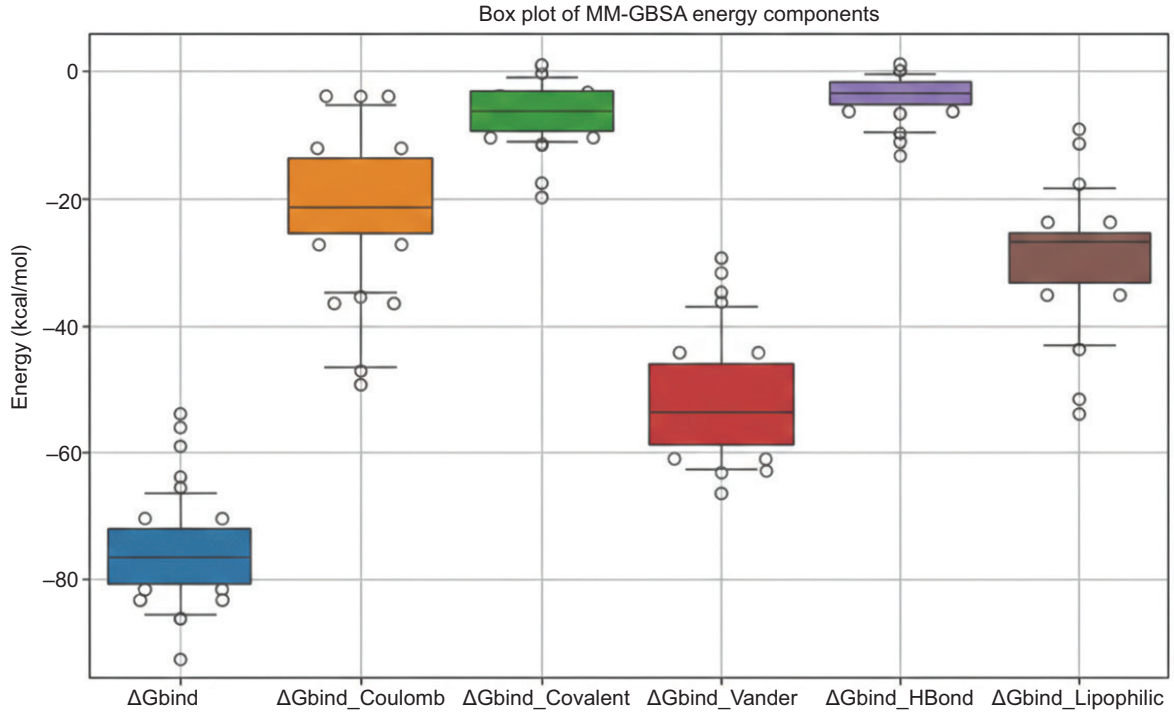

Figure 12. Molecular Mechanics–Generalized Born Surface Area (MM-GBSA) binding free energy analysis of the coumarin–COMT complex. The figure represents total binding free energy (ΔG_bind) along with individual energy contributions, including van der Waals (ΔG_vdW), electrostatic (ΔG_coulomb), lipophilic, and hydrogen bonding terms, indicating the dominant forces stabilizing the complex.

force. Electrostatic stabilization is moderate (ΔG_coulomb = −20.32 ± 4.79 kcal/mol), while hydrogen bonding contributes modestly (ΔG_Hbond = −2.01 ± 1.02 kcal/mol). The covalent/strain-related term is small (ΔG_covalent = −4.91 ± 2.00 kcal/mol), implying limited internal penalty. The overall ΔGbind value of −75.19 kcal/mol shows a less negative value than the total of its favorable components because there exist positive terms that are typically associated with solvation/desolvation and related penalties that were not included in this summary. The positive terms not included in this summary, together with the strong vdW/lipophilic stabilization effects, work to create a partial cancellation.

4. DISCUSSION

The enzyme COMT plays an essential role in dopaminergic metabolism by catalyzing the methylation of catechol substrates, leading to dopamine degradation in brain tissue. This process is particularly important in PD, where dopamine levels are significantly reduced. Therefore, COMT inhibitors are clinically used as adjuncts with L-DOPA to enhance dopamine availability and improve motor function in PD patients (Kalia & Lang, 2015; Männistö & Kaakkola, 1999).

In the present study, an ***in silico*** **approach** was employed to evaluate MP phytoconstituents as potential COMT inhibitors using molecular docking, molecular dynamics (MD) simulations, and MM–GBSA binding free energy analysis. The docking results revealed that several phytochemicals exhibited a stronger predicted binding affinity toward COMT than the co-crystallized ligand and the reference drug. Among the evaluated compounds, coumarin demonstrated the highest docking score (–7.6 kcal/mol), followed by linoleic acid, oleic acid, and myristic acid. These findings support the presence of bioactive constituents in MP, which are capable of modulating COMT activity, thereby supporting its traditional use in the management of PD (Bonifácio et al., 2007; Rai et al., 2020).

The co-crystallized ligand formed multiple hydrogen bonds within the active site; however, it exhibited a lower docking score (–5.2 kcal/mol) compared to the phytoconstituents. This highlights an important principle in structure-based drug design: hydrogen bonding alone does not determine binding strength. Instead, ligand stabilization within enzyme catalytic pockets depends on a combination of interactions, including hydrophobic packing, π–π stacking, dispersion forces, and ionic interactions (Bissantz et al., 2010; Davis & Teague, 1999).

4.1. Enhanced structural and dynamic validation of coumarin

The majority of existing research on coumarin has primarily focused on enzyme inhibition or synthetic derivatives evaluated through *in vitro* biochemical assays, often lacking detailed structural and dynamic validation (Foroozesh et al., 2019; Zhao et al., 2021). The present study utilized the COMT crystal structure (PDB ID: 6I3D) to demonstrate that naturally derived coumarin binds directly to key catalytic residues, including Trp143 and Ile91, indicating target-specific inhibition.

The observed binding affinity (–7.6 kcal/mol) is comparable to or higher than previously reported natural COMT inhibitors (Sherif et al., 2024), suggesting a strong interaction within the enzyme active site. Furthermore, MD simulations revealed stable protein–ligand interactions (RMSD: 1.3–1.6 Å), with sustained binding supported by hydrogen bonding, hydrophobic interactions, and water-mediated contacts involving Glu90.

Additionally, MM–GBSA binding free energy calculations demonstrated a favorable binding energy (–75.19 ± 4.96 kcal/mol), primarily driven by van der Waals and lipophilic interactions. This thermodynamic validation provides novel insight into the binding strength of coumarin with COMT, which has not been extensively reported in earlier studies. Collectively, these findings highlight that naturally derived coumarin exhibits strong binding affinity, dynamic stability, and favorable energetic properties.

4.2. Coumarin as a complementary agent to L-DOPA

Although L-DOPA remains the gold standard for PD treatment due to its role as a dopamine precursor, its therapeutic efficacy is limited by rapid metabolism, particularly by COMT. This limitation underlies the clinical use of COMT inhibitors such as entacapone to prolong L-DOPA action.

In this context, coumarin does not act as a substitute for L-DOPA but instead functions through a complementary mechanism of action. The present findings indicate that coumarin acts as a potential COMT inhibitor, thereby reducing dopamine degradation and preserving both endogenous and exogenously administered dopamine. This may enhance dopaminergic neurotransmission and improve therapeutic outcomes.

Thus, coumarin may improve the pharmacokinetic profile of L-DOPA while maintaining its pharmacodynamic effects. Its therapeutic relevance lies in its potential to prolong L-DOPA action and reduce associated side effects, positioning it as a supportive phytoconstituent rather than a replacement therapy.

4.3. Synergistic contribution of phytoconstituents

The docking results further demonstrated that coumarin exhibited the highest binding affinity among the studied compounds, confirming it as the primary contributor to COMT inhibition. Coumarin showed direct interaction with key active site residues (Trp143 and Ile91), along with stable hydrogen bonding and hydrophobic interactions during MD simulations.

In contrast, linoleic acid and myristic acid, being long-chain fatty acids, primarily contributed through hydrophobic interactions within the enzyme binding pocket. Although their binding affinities were slightly lower, they likely enhance ligand stabilization by increasing the hydrophobic environment, thereby supporting the overall stability of the protein–ligand complex.

This indicates a synergistic mode of action, where multiple phytoconstituents collectively enhance therapeutic efficacy. In MP, this synergy may involve dopamine restoration via L-DOPA along with inhibition of dopamine degradation through compounds such as coumarin.

Supporting literature suggests that coumarin derivatives from plants such as *Angelica archangelica* and *Ferula* species exhibit neuroprotective and enzyme inhibitory activities (Venugopala et al., 2013). Additionally, linoleic acid has been reported to possess anti-inflammatory and neuroprotective effects in PD models (Koppula et al., 2012), while fatty acids such as myristic acid contribute indirectly through membrane stabilization and cellular signaling.

Overall, these findings establish that coumarin serves as the primary driver of COMT inhibitory activity, while linoleic acid and myristic acid contribute through synergistic stabilization and supportive interactions.

5. CONCLUSION

The current research applied an *in silico* methodology, which combined molecular docking with MD simulation and MM–GBSA binding free energy assessment to assess the COMT inhibitory activity of MP phytoconstituents. Among the tested compounds, coumarin exhibited the strongest binding capacity while maintaining stable contacts with crucial active site residues (Trp143 and Ile91) because of its binding energy and dynamic stability during the complete simulation time. The findings indicate that coumarin functions as an effective natural scaffold that can be used by scientists to develop COMT inhibitors.

The results show that coumarin functions as a treatment that complements L-DOPA therapy by blocking dopamine degradation, thereby boosting dopaminergic

neurotransmission, which improves PD treatment results. The protein–ligand complex stability arises from the combined hydrophobic interactions of linoleic and myristic acids and other phytoconstituents.

The study results rely entirely on computational prediction methods. The research lacks both *in vitro* enzymatic assays and *in vivo* validation, which is a major limitation. Also, the researchers did not conduct any experiments to assess the pharmacokinetics, bioavailability and toxicity of the compounds they identified in their study.

The COMT inhibitory activity, together with the therapeutic potential of coumarin and other phytoconstituents from MP, requires experimental studies, which must include biochemical inhibition assays and animal models. The study establishes a theoretical base for creating plant-based COMT inhibitors while providing evidence that supports the use of MP in treating PD.

ORCID

Mohmmad Qutboddin 0009-0001-7627-9445
Syed Sagheer Ahmed 0000-0001-9817-9747
Bharathi D R 0000-0002-8153-2839

AUTHOR CONTRIBUTIONS

Mohmmad Qutboddin: Research concept and design, Collection and/or assembly of data, Data analysis and interpretation, Writing the article. Syed Sagheer Ahmed: Critical revision and final approval of the article. Bharathi D.R.: Data analysis and interpretation.

CONFLICTS OF INTEREST

The authors declare that there is no conflict of interest.

FUNDING

Not available.

REFERENCES

Balestrino, R., Schapira, A.H.V., 2020. Parkinson disease. European Journal of Neurology. 27(1), 27–42. https://doi.org/10.1111/ene.14108

Berman, H.M., Westbrook, J., Feng, Z., Gilliland, G., Bhat, T.N., Weissig, H., Shindyalov, I. N., Bourne, P.E., 2000. The protein data bank. Nucleic Acids Research. 28(1), 235–242. https://doi.org/10.1093/nar/28.1.235

Bissantz, C., Kuhn, B., Stahl, M., 2010. A medicinal chemist's guide to molecular interactions. Journal of Medicinal Chemistry. 53(14), 5061–5084. https://doi.org/10.1021/jm100112j

Bloem, B.R., Okun, M.S., Klein, C., 2021. Parkinson's disease. The Lancet. 397(10291), 2284–2303. https://doi.org/10.1016/S0140-6736(21)00218-X

Bonifácio, M.J., Palma, P.N., Almeida, L., Soares-da-Silva, P., 2007. Catechol-O-methyltransferase and its inhibitors in Parkinson's disease. CNS Drug Reviews. 13(3), 352–379. https://doi.org/10.1111/j.1527-3458.2007.00018.x

Bowers, K.J., Chow, E., Xu, H., Dror, R.O., Eastwood, M.P., Gregersen, B.A., Klepeis, J.L., Kolossváry, I., Moraes, M.A., Sacerdoti, F.D., Salmon, J.K., Shan, Y., Shaw, D.E., 2006. Scalable algorithms for molecular dynamics simulations on commodity clusters. Proceedings of the ACM/IEEE Conference on Supercomputing. https://doi.org/10.1145/1188455.1188544

Davis, A.M., Teague, S.J., 1999. Hydrogen bonding, hydrophobic interactions, and failure of the rigid receptor hypothesis. Angewandte Chemie International Edition. 38(6), 736–749. https://doi.org/10.1002/(SICI)1521-3773(19990315)38:6<736::AID-ANIE736>3.0.CO;2-7

Dorsey, E.R., Sherer, T., Okun, M.S., Bloem, B.R., 2018. The emerging evidence of the Parkinson pandemic. Journal of Parkinson's Disease. 8(s1), S3–S8. https://doi.org/10.3233/JPD-181474

Foroozesh, M., Primrose, G., Guo, Z., Bell, L.C., Alworth, W.L., Guengerich, F.P., 2019. Aryl coumarins: a new class of inhibitors of cytochrome P450 enzymes. Journal of Medicinal Chemistry. 62(3), 1176–1193. https://doi.org/10.1021/acs.jmedchem.8b01664

GBD 2021 Parkinson's Disease Collaborators, 2024. Global, regional, and national burden of Parkinson's disease, 1990–2021. The Lancet Neurology. https://doi.org/10.1016/S1474-4422(24)00010-8

Hettiarachchi, D.S., Gunathilake, K.D.P.P., 2023. Nutritional and medicinal properties of *Mucuna pruriens*. Journal of Food Composition and Analysis. 115, 104920. https://doi.org/10.1016/j.jfca.2022.104920

Hollingsworth, S.A., Dror, R.O., 2018. Molecular dynamics simulation for drug discovery. Neuron. 99(6), 1129–1143. https://doi.org/10.1016/j.neuron.2018.08.011

Horsager, J., Andersen, K.B., Knudsen, K., Skjærbæk, C., Fedorova, T.D., Okkels, N., Schaeffer, E., Bonkat, S.K., Geday, J., Otto, M., Sommerauer, M., Danielsen, E.H., Bech, E., Kraft, J., Munk, O.L., Hansen, S.D., Pavese, N., Göder, R., Brooks, D.J., Berg, D., Borghammer, P., 2020. Brain-first versus body-first Parkinson's disease: a multimodal imaging case-control study. Brain. 143(10), 3077–3088. https://doi.org/10.1093/brain/awaa238

Kalia, L.V., Lang, A.E., 2015. Parkinson's disease. The Lancet. 386(9996), 896–912. https://doi.org/10.1016/S0140-6736(14)61393-3

Katzenschlager, R., Evans, A., Manson, A., Patsalos, P.N., Ratnaraj, N., Watt, H., Timmermann, L., Van der Giessen, R., Lees, A.J., 2004. *Mucuna pruriens* in Parkinson's disease. Journal of Neurology, Neurosurgery & Psychiatry. 75(12), 1672–1677. https://doi.org/10.1136/jnnp.2003.028761

Koppula, S., Kumar, H., More, S.V., Kim, I.S., Choi, D.K., 2012. Neuroprotective potential of antioxidants in Parkinson's disease. International Journal of Molecular Sciences. 13(9), 10608–10629. https://doi.org/10.3390/ijms130910608

Lampariello, L.R., Cortelazzo, A., Guerranti, R., Sticozzi, C., Valacchi, G., 2012. The magic velvet bean of *Mucuna pruriens*.

Journal of Traditional and Complementary Medicine. 2(4), 331–339. https://doi.org/10.1016/S2225-4110(16)30119-5

Lev, N., Melamed, E., Offen, D., 2003. Apoptosis and Parkinson's disease. Progress in Neuro-Psychopharmacology & Biological Psychiatry. 27(2), 245–250. https://doi.org/10.1016/S0278-5846(03)00006-6

Lionta, E., Spyrou, G., Vassilatis, D.K., Cournia, Z., 2014. Structure-based virtual screening. Current Topics in Medicinal Chemistry. 14(16), 1923–1938. https://doi.org/10.2174/1568026614666140929124445

Lipinski, C.A., Lombardo, F., Dominy, B.W., Feeney, P.J., 2001. Experimental and computational approaches. Advanced Drug Delivery Reviews. 46(1–3), 3–26. https://doi.org/10.1016/S0169-409X(00)00129-0

Männistö , P.T., Kaakkola, S., 1999. COMT: biochemistry and clinical efficacy of the new selective COMT inhibitors. Pharmacological Reviews. 51(4), 593–628.

Manyam, B.V., 1995. *Mucuna pruriens* in Parkinson's disease. Journal of Alternative and Complementary Medicine. 1(3), 249–255.

Mohanraj, K., Vivek-Ananth, R.P., Karthikeyan, B.S., Bharath Chand, R.P., Aparna, S.R., Mangalapandi, P., Samal, A., 2018. IMPPAT database. Scientific Reports. 8, 4329. https://doi.org/10.1038/s41598-018-22631-z

Poewe, W., Seppi, K., Tanner, C.M., Halliday, G.M., Brundin, P., Volkmann, J., Schrag, A.E., Lang, A.E., 2017. Parkinson disease. Nature Reviews Disease Primers. 3, 17013. https://doi.org/10.1038/nrdp.2017.13

Rai, S.N., Birla, H., Singh, S.S., Zahra, W., Patil, R.R., Jadhav, J.P., Gedda, M.R., Singh, S.P., 2020. *Mucuna pruriens* in Parkinson's disease. Frontiers in Aging Neuroscience. 12, 593786. https://doi.org/10.3389/fnagi.2020.593786

Sathiyanarayanan, L., Arulmozhi, S., 2007. *Mucuna pruriens* review. Pharmacognosy Reviews. 1(1), 157–162.

Sherif, S., Sameh, A., Salah, S.M., Omar, A., Elhaes, H., Ibrahim, A., Ibrahim, M.A., 2024. DFT and QSAR study of catechol-O-methyltransferase (COMT) inhibitors for Parkinson's disease treatment. Optical and Quantum Electronics. 56, 633. https://doi.org/10.1007/s11082-023-06125-5

Singh, S., Dikshit, M., 2007. Apoptotic neuronal death. Indian Journal of Experimental Biology. 45(9), 705–715.

Spillantini, M.G., Schmidt, M.L., Lee, V.M., Trojanowski, J.Q., Jakes, R., Goedert, M., 1997. Alpha-synuclein in Lewy bodies. Nature. 388(6645), 839–840. https://doi.org/10.1038/42166

Trott, O., Olson, A.J., 2010. AutoDock Vina. Journal of Computational Chemistry. 31(2), 455–461. https://doi.org/10.1002/jcc.21334

Venugopala, K.N., Rashmi, V., Odhav, B., 2013. Natural coumarin derivatives. BioMed Research International. 2013, 963248. https://doi.org/10.1155/2013/963248

Wong, Y.C., Krainc, D., 2017. Alpha-synuclein toxicity. Nature Medicine. 23(2), 1–13. https://doi.org/10.1038/nm.4269

Zhao, H. , Neamati, N., et al., 2021. Coumarin derivatives. European Journal of Medicinal Chemistry. 209, 112939. https://doi.org/10.1016/j.ejmech.2020.112939